Supplementary Information

Interior geometry reconstructs the sarcophagus envelope and exterior slope of the Great Pyramid of Khufu

Lucas Giovani Ribeiro and Marcos André Simonssini

npj Heritage Science

Part	Contents	PDF pages
I	Supporting information Sections S1–S25, Tables S1–S17 and Figures S1–S4	2–19
II	Frozen prospective envelope protocol Protocol A	20–22
III	Frozen prospective original position protocol Protocol B	23–24

Part I retains the S section, figure, table and equation labels used in the manuscript. The original page numbers in Part I are retained; the page ranges above refer to this combined PDF.

Protocols A and B are reproduced unchanged, including their freeze dates, version labels, numerical bands and decision rules. They are prospective specifications and have not been executed on new survey observations. Their historical references to versioned files are resolved in Supplementary Data 1.

Supplementary Data 1 is supplied separately as a ZIP archive containing the scientific code, frozen inputs, machine-readable outputs, protocol records and execution instructions.

Supplementary Information, Part I Supporting information

Interior geometry reconstructs the sarcophagus envelope and exterior slope of the Great Pyramid of Khufu

HOW TO READ THIS SUPPLEMENT

Sections S1–S4 give the reversible decoder and its outputs. Sections S5–S9 document the five-panel R10.1 specificity audit and R11 exact null. Section S9A gives the supplementary historical volume-balance check. Sections S10–S17 retain the inverse, sensitivity, control and prospective analyses, and S18–S20 provide the executable inventory and claim map. Section S21 documents the retrospective joint reconstruction and dependency audit; S22 extends the rule grammar to joint reconstruction; S23 records the reconstruction and registration audit; and S24 documents the whole-grammar Hawara control and lid-reference interval. Section S25 reports the exploratory grammar expansion and bounded-input ranking audit R17.

A REVERSIBLE PRIMARY CONSTRUCTION

S1. Measurement inventory and evidential roles

Table S1. Measurement provenance and roles

Quantity	Symbol	Value	Role
West-wall top width	W	206.04 in (5.233416 m)	preserved internal input
Mean chamber width	Wmean	206.12 in (5.235448 m)	role sensitivity
Free floor-to-ceiling height	H	230.09 in (5.844286 m)	preserved internal input
External sarcophagus height	h	41.31 in (1.049274 m)	preserved internal input
Current external length	Lcurrent	89.62 in (2.276348 m)	damaged-state control
Original external length	L0	approximately 90.60 in (≈2.301240 m)	withheld morphology
Mean exterior base	B	9068.8 in (230.34752 m)	downstream scale check
North-face inclination	thetaN	51°50′40″ ±1′05″	downstream angle check
Mean present transverse correction	δ current	9.64875 in (0.245078250 m)	position ablation
Original transverse offset	delta0	unrecovered	prospective endpoint
External sarcophagus width	W_e	38.50 in (0.977900 m)	supplementary R12/R13 input
Internal cavity length	l_i	78.06 in (1.982724 m)	supplementary R12/R13 input
Internal cavity width	w_i	26.81 in (0.680974 m)	supplementary R12/R13 input
Internal cavity depth	d_i	34.42 in (0.874268 m)	supplementary R12/R13 input

The photograph that motivated the study is illustrative only. Every result below is calculated from an orthographic section and documented dimensions. Petrie's reconstructed 90.60-in envelope is not inserted into the internal decoder.

Primary architectural quantities derive from Petrie (1883), exterior size and orientation checks from Cole (1925) and Nell and Ruggles (2014), and Hawara dimensions from Petrie (1890). The 14/11 historical background follows Gillings (1972), Robins and Shute (1987), and Rossi (2004).

S2. Orthographic X and the primitive equality

Let the chamber section have width W and free height H. Let the centred original sarcophagus envelope have length L and external height h. Set G=H-h. The crossed branches from the upper chamber corners to the opposite upper sarcophagus corners intersect at the chamber centreline. Similar triangles give the lower rise D and upper rise U:

$$\mathrm{D} = \mathrm{GL}/(\mathrm{W}+\mathrm{L}), \qquad \mathrm{U} = \mathrm{GW}/(\mathrm{W}+\mathrm{L}), \qquad \mathrm{g} = (\mathrm{W}\text{-}\mathrm{L})/2. \qquad (\mathrm{S1})$$

The reverse-engineered primitive instruction is the parameter-free equality between the lower vertical rise and either one-sided lateral gap:

$$\mathrm{D} = \mathrm{g}. \qquad (\mathrm{S2})$$

Substitution yields a quadratic with one positive physical root:

$$\mathrm{L_Dg} = \mathrm{sqrt}((\mathrm{H}\text{-}\mathrm{h})\hat{}2 + \mathrm{W}\hat{}2) - (\mathrm{H}\text{-}\mathrm{h}). \qquad (\mathrm{S3})$$

In dimensionless form, with A=(H-h)/W and r_Dg=L_Dg/W, the mapping is reversible:

$$\mathrm{A} = (1\text{-}\mathrm{r_Dg}\hat{}2)/(2\mathrm{r_Dg}), \qquad \mathrm{r_Dg} = \mathrm{sqrt}(1+\mathrm{A}\hat{}2)\text{-}\mathrm{A}. \qquad (\mathrm{S4})$$

The lower profile tangent then follows without exterior input:

$$\tan(\mathrm{theta_Dg}) = (\mathrm{W}\text{-}\mathrm{L_Dg})/\mathrm{L_Dg} = (1\text{-}\mathrm{r_Dg})/\mathrm{r_Dg}. \qquad (\mathrm{S5})$$

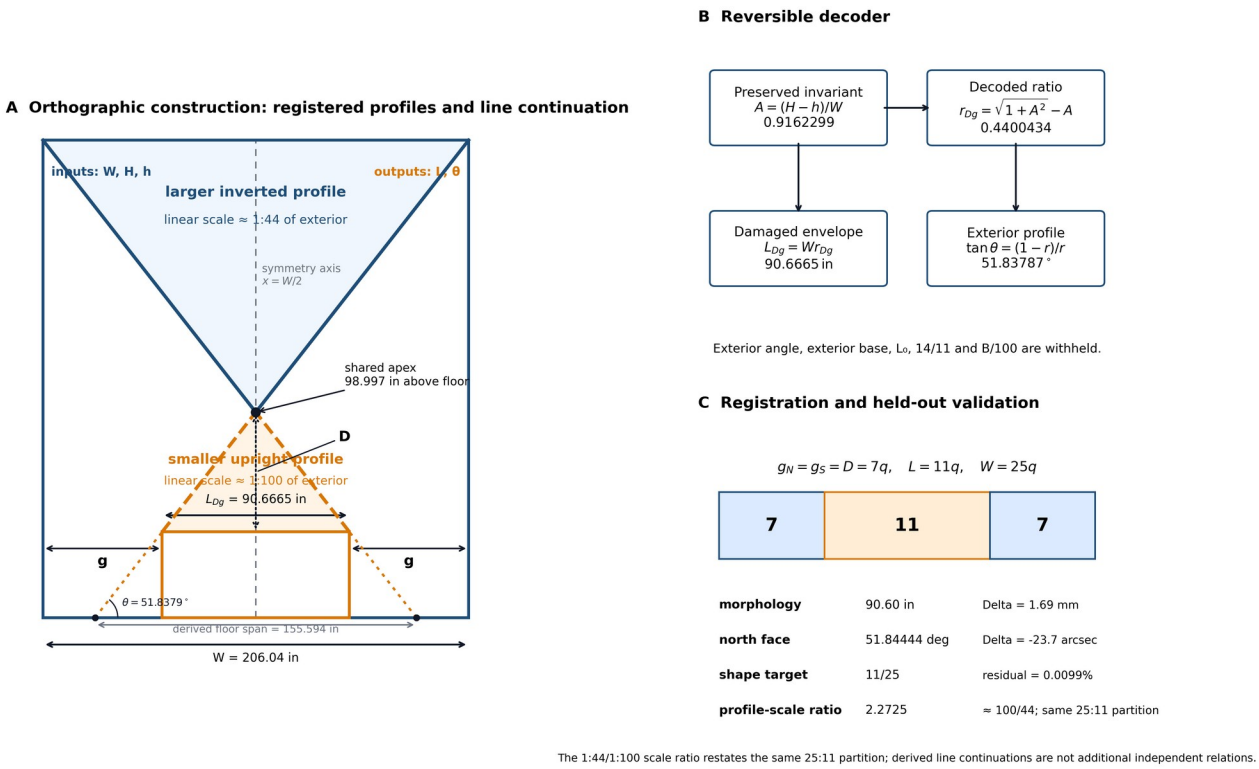


Figure S1. Reversible internal dimensional code, registered profiles and dependent line continuations. Preserved W, H and h generate r_Dg, L_Dg and the lower profile; g_N=g_S=D registers the same module in two horizontal directions and one vertical direction. The smaller upright profile is approximately 1:100 of the exterior profile, the larger inverted chamber-width profile is approximately 1:44, and both share an apex 98.997 in above the floor. Continued beyond the sarcophagus corners, the same lines intersect the floor at x=25.223 and 180.817 in, giving a derived 155.594-in span. Relative to the intrinsic symmetry axis x=W/2, the registered and derived regions expose eight drawable right-triangle manifestations of the same 51.8379° line direction; some are nested, all are geometrically dependent, and none is counted as an additional relation. The 1:44/1:100 scale ratio is the same 25:11 partition and is not an additional independent relation. Exterior quantities enter only downstream. Source: authors' calculations.

S3. Numerical decoder output

Table S2. Decoder outputs and downstream checks

Output	Value	Interpretation
A=(H-h)/W	0.916229858	preserved W,H,h only
r_Dg=sqrt(1+A²)-A	0.440043401	D=g-derived length ratio
L=Wr	90.666542 in	1.69 mm above rounded morphology 90.60 in
theta=atan((1-r_Dg)/r_Dg)	51.837871°	−23.7 arcsec from north-face value
r_Dg vs 11/25	0.00986%	specific dimensional target
B/W	44.014754	approximately 44
B/L	100.023667	approximately 100
L_V=2V_c/(W_eh)	90.583750 in	historical volume-balance inverse; 0.41 mm from morphology; R12 non-scored

The rounded historical morphology is a retrodictive check, not a precision-calibrated uncertainty distribution. The 1.69-mm central difference is reported descriptively. A new blinded morphometric interval is required to quantify discrimination.

S4. Form, position and scale registration

For the ideal ratio r_Dg=11/25, centring gives g/W=(1-r_Dg)/2=7/25. Under D=g, D/W=7/25 and the lower profile has total base:height 11:7, or rise/run 14:11. The display 7|11|7 is a redundant manifestation of one relation, not three independent coincidences.

Petrie had already discussed h/W≈1/5. This supplies vertical registration but is not a novel isolated ratio. The exterior scale B/W≈44 is consistent with two cubit counts and therefore has a strong shared-metrology explanation when considered alone. Its role in the present construction is as a scale-registration layer: once L/W=11/25 and B/W=44 are introduced, B/L=100 follows algebraically and is not counted as an independent channel. In the orthographic section this same network appears visually as two similar profiles with a common apex at 98.997 in above the floor: the smaller profile is upright at approximately 1:100, while the larger chamber-width profile is inverted at approximately 1:44. Their ratio W/L_Dg≈100/44 is simply the 25:11 transverse partition expressed as a scale ratio, not a new independent correspondence.

The same two lines can be continued to the floor without introducing any new fitted quantity. With the left boundary of the transverse section as x=0, the intercepts are x=25.223154 and 180.816846 in, so the floor span is 155.593692 in. The apex height is h+D=98.996729 in, and the one-sided floor half-span is 77.796846 in; their ratio reproduces tan(theta_Dg)=1.272503. The lateral regions between each floor intercept and the adjacent sarcophagus side have horizontal run 32.463575 in and vertical rise h=41.31 in, again reproducing the same line direction. Relative to the intrinsic symmetry axis x=W/2, the registered and derived regions expose eight readily drawable right-triangle manifestations, with some regions nested. This is a visualisation of one two-line geometry, not eight observations.

For a descriptive axis-rotation check, retain H, h and the decoded L_Dg but replace W in the crossed-corner Equation (1) by Petrie's 412.24-in chamber length. The result is theta_long=atan[2(H-h)/(412.24+L_Dg)]=36.8976 degrees, a 41.0% slope departure from tan(theta_Dg). This is not an additional scored R10.1 channel. It shows that the interior closure is transverse-specific even though the recovered profile is the inclination of a vertical section normal to a face and, in ideal symmetric square-pyramid geometry, is common to all four exterior faces. This dimensional-substitution check is distinct from the legacy physical rotated-axis crossed-corner control in S12, which uses the coffer's orthogonal external width and gives approximately 39.95 degrees; both fail to reproduce the exterior profile.

$$\mathrm{B/L} = (\mathrm{B/W})/(\mathrm{L/W}) = 44/(11/25) = 100. \qquad \text{(S6)}$$

$$\mathrm{B}/44 = \mathrm{B}/100 + 2\mathrm{Z}/100, \text{ for B:Z} = 440{:}280. \qquad \text{(S7)}$$

The operational definition used in the manuscript is therefore: dimensional encoding is reversible compression of relations of form, position and scale into a smaller set of invariants and geometric instructions.

B CORRECTED FIVE-PANEL SPECIFICITY AUDIT (R10.1)

S5. Frozen grammar and corrections from R10

R10.1 preserves the original frozen grammar, domains, targets, tolerances and random seed 21, while correcting three implementation or labelling defects. Exact grid roots are retained, increasing the physical-root total from 459 to 476 and the distinct-class total from 126 to 127. The position criterion is explicitly max(|g_N-D|,|g_S-D|)≤tol·g. The 5.936-fold runner-up margin is labelled a descriptive worst-channel ranking, max(e_L,e_theta), rather than an inferential statistic.

The grammar generated 1,950 expressions from low-complexity segment relations. Sixteen tautologies and 229 expressions without L dependence were excluded. Numerical and exact-grid roots were restricted to 30<L<W−30 in (30<L<176.04 in for the reference width) and collapsed by predicted L into algebraic solution classes.

S6. Panel 1 — rule uniqueness

Table S3. Rule grammar counts

Quantity	R10.1 result
Generated expressions	1950
Tautological exclusions	16
L-independent exclusions	229
Physical roots	476
Distinct classes	127
Classes passing both criteria at 0.2% (also length alone)	1
Equivalent expressions in winning class	13

Table S4. Leading distinct rule classes

L prediction (in)	eL	eθ	Equivalent rules	Example
90.666542	0.073446%	0.023614%	13	D = g
90.995	0.435982%	0.134167%	1	H = 2(W − L)
90.054325	0.60229%	0.183101%	5	G = L + Y
88.144697	2.710048%	0.833415%	1	U = L/2 + L
94.39	4.183223%	1.262698%	6	2L = G

Only D=g recovers length within 0.2%. Three classes pass the tangent threshold and one passes both; the length and joint selections are identical. The runner-up H=2(W−L) gives L=90.995 in, eL=0.435982% and eθ=0.134167%. The 5.936-fold worst-channel margin is descriptive. S21 diagnoses the dependency while retaining the frozen scoring specification and all class results.

S7. Panel 2 — plausible-geometry null

Table S5. Specific and generic rational targets

Relative tolerance	Specific r=11/25	Any reduced rational, denominator ≤30
0.1%	0.5417%	24.3453%
0.2%	1.0828%	47.2940%
0.5%	2.6975%	81.4195%
1.0%	5.3712%	93.2295%

The null draws W uniformly from 150–280 in, H/W uniformly from 0.9–1.4 and h/W uniformly from 0.15–0.30, then applies the same D=g decoder. At the frozen 0.2% tolerance, the specific 11/25 target occupies 1.0828% of 400,000 valid draws, while the broad class of simple rational targets occupies 47.2940%. R11 integrates the induced A=(H/W)-(h/W) density over the same frozen target interval and gives 1.0850945%, independently verifying the simulation without a random seed. These are conditional frequencies under the declared null, not universal probabilities. Under D=g, r and theta are linked and are not counted as independent hits.

S8. Panels 3 and 4 — physical roles and position

Table S6. Leading physical-role assignments

W role	H role	h role	L	theta	eL %	eθ %
west-wall top width	free floor-to-ceiling	coffer external height	90.6665	51.8379	0.0734	0.0236
mean chamber width	free floor-to-ceiling	coffer external height	90.7255	51.8248	0.1386	0.0704
mean chamber width	full wall height	coffer external height	89.092	52.7184	1.6645	3.2025
west-wall top width	full wall height	coffer external height	89.0337	52.7314	1.7288	3.2508
mean chamber width	free floor-to-ceiling	cavity internal depth	88.5345	53.0225	2.2798	4.3469
west-wall top width	free floor-to-ceiling	cavity internal depth	88.4765	53.0354	2.3438	4.3958

Two of 32 assignments close at 0.5%; they are the west-wall top width and chamber mean width with the same free height and external sarcophagus height. The third assignment already has a 3.2025% tangent residual. Thus the closing depends on the correct physical measurement class, not merely on selecting any chamber and sarcophagus dimensions.

Table S7. Transverse positional tolerances

Triple-register tolerance	Accepted centre semiwindow	As % of total free span
0.1%	1.47 mm	0.05%
0.5%	7.33 mm	0.25%
1.0%	14.65 mm	0.5%
5.0%	73.26 mm	2.5%

At 1% of the one-sided gap, the accepted centre displacement is ±14.65 mm; the full accepted width is 29.30 mm. Petrie’s mean present-position correction of 245.1 mm is 16.7 times the semiwindow. This R10.1 registration window is a structural-specificity diagnostic and does not replace the separately frozen archaeological position protocol.

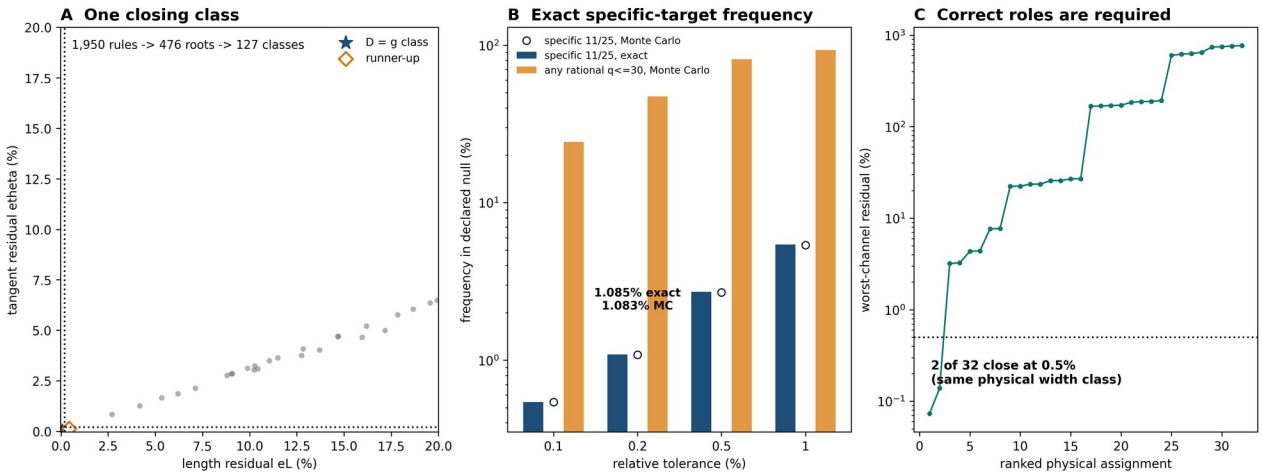


Figure S2. Specificity audit and exact-null verification. The rule grammar identifies one closing class at 0.2%; exact integration verifies the frozen Monte Carlo frequency for the specific 11/25 target; the role panel shows dependence on the correct physical measurement class. The length criterion alone selects the same class; the dependent tangent filter adds no rejection. Source: authors' calculations.

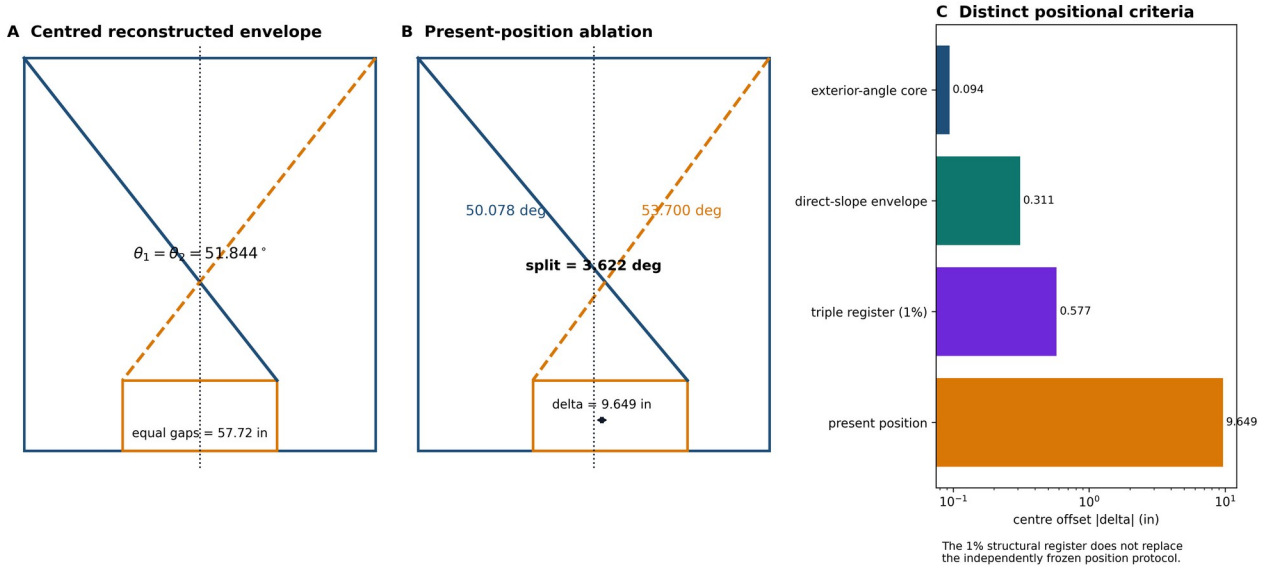


Figure S3. Exact-coordinate position ablation. A centred reconstructed envelope gives two 51.844° branches. Petrie's present-position correction gives 50.078° and 53.700°, a 3.622° split. The panels use equal data aspect. Source: authors' calculations.

S9. Panel 5 — comparative and operator-transfer controls

Table S8. Comparative and operator-transfer controls

Case	Control type	D=g L	D=g theta	Target	Tangent residual
Khufu King's Chamber	coffer preserved	90.667	51.838	51.84	-0.02%
Queen's Chamber (N/S wall top)	operator transfer: no coffer preserved	107.577	42.412	51.84	-28.23%
Queen's Chamber (gable apex)	operator transfer: no coffer preserved	85.873	54.407	51.84	9.77%

Case	Control type	D=g L	D=g theta	Target	Tangent residual
Hawara (transverse, corrected)	homologous comparative control	64.269	24.972	48.75	-59.16%

Hawara is the homologous chamber–coffer control because Petrie documented a transversely centred sarcophagus. Its correct transverse values are W=94.2 in, H=92.4 in, h=55.5 in and actual L=48.4 in. The observed crossed-corner angle is 27.363°, while the D=g transfer predicts L=64.269 in and theta=24.972°. Both are far from the selected casing-fragment target near 48.75°, which Petrie himself regarded as not securely fixed. A longitudinal-axis calculation gives 11.18°, but it is not a homologous test because Petrie's documented centring applies transversely.

The Queen's Chamber has no preserved coffer and is therefore not a homologous control. Its wall-top and gable-apex calculations are operator-transfer tests. The finished gable angle near 30.50° remains a same-monument triangularity control: internal triangular architecture does not automatically reproduce the exterior face.

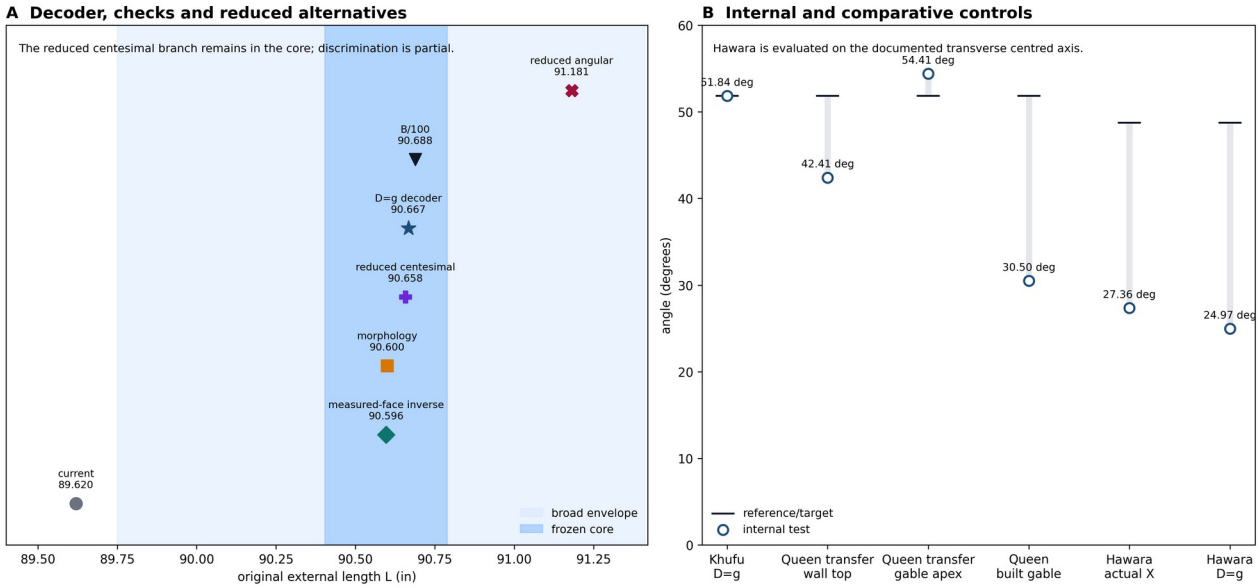


Figure S4. Downstream compatibility and corrected controls. Panel A preserves the R09 conclusion of partial discrimination. Panel B distinguishes Queen's Chamber operator transfers from the corrected transverse Hawara control. Source: authors' calculations.

C SUPPLEMENTARY HISTORICAL COFFER-VOLUME CHECK (R12)

S9A. Historical volume-balance check (R12)

Petrie's §61 mean-plane values are contents 72,030 in³, solid bulk 70,500 in³ and total 142,530 in³; in §156 he explicitly called the near equality of contents and solid bulk inexact and rejected transcendent accuracy for it. Using the published mean dimensions gives $V_c=l_iw_id_i$=72,033.7836 in³. At L=89.62 in the corresponding rectilinear granite volume is 70,501.0011 in³ and total envelope volume is 142,534.7847 in³, reproducing Petrie's three mean-plane figures to 3.8, 1.0 and 4.8 in³. This validates the implementation before any reconstruction is introduced. Imposing the historical ideal $V_c=V_g$ gives $L_V=2V_c/(W_eh)$=90.5837505 in, 0.41 mm below Petrie's morphology envelope and 2.10 mm below L_Dg.

At the surviving mean external length 89.62 in, cavity/granite=1.021741 (+2.1741%). At Petrie's morphology envelope L0=90.60 in, cavity/granite=0.999641, only 0.035864% from exact balance. At L_Dg, cavity/granite=0.998175 (−0.182463%). Thus the historical 1,530-in³ mean-plane imbalance is almost cancelled, under the same rectilinear approximation, by restoring the separately inferred missing envelope. A secondary bounded-domain sensitivity integrates the allowable external-width interval analytically and uses 64-point Gauss–Legendre quadrature over l_i,w_i,b. At the

D=g-state residual of 0.182463%, the declared domain gives 0.440013%, spanning 0.312267–0.730998% across narrow/declared/wide domains. These are conditional sensitivity frequencies only; the evidential point of R12 is the historically pre-existing criterion and its reconstruction of L, not a universal p-value.

D RETAINED R01–R09 ANALYSES

S10. Measured-face inverse and bounded sensitivity (R01)

As a downstream validation route, the exterior angle can be used in the inverse direction:

$$\mathrm{L_theta} = 2(\mathrm{H\text{-}h})/\tan(\mathrm{theta_face}) - \mathrm{W}. \qquad (S8)$$

Using the measured north-face inclination gives 90.596476642 in. The angle-only inverse range is 90.404–90.789 in. Combining the declared historical variations in W, H, h and theta gives the broad envelope 89.750–91.412 in. These ranges are bounded sensitivities, not Gaussian confidence intervals.

S11. Exterior scale checks and information accounting (R04, R09)

The historically specified B/100 check gives 90.688 in. Under the D=g architecture it is a downstream scale consequence rather than an independent probability channel. It remains useful as a consistency check based on a distinct exterior measurement.

R09 enforces target-consistent comparisons. On Petrie's measured-face scale, the internal measured inverse is 90.596476642 in and the reduced H/W,h/W angular inversion is 91.180577783 in, separated by 14.836 mm. Under exact 14/11 the corresponding pair is 90.614285714 and 91.198421923 in. Comparing 90.596 with 91.198 mixes conventions and is not used.

The reduced angular branch lies outside the frozen compatibility core but inside the broad envelope. The reduced centesimal branch L=0.44W=90.6576 in remains inside the core. Hence the existing protocol has partial directional discrimination and does not exclude the complete reduced proportional family.

S12. State, orientation and boundary controls (R05–R07)

Table S9. Retained state and boundary controls

Control	Design	Result
Rotated axis	Chamber length paired with coffer width	approximately 39.95°; fails exterior profile
Current damaged length	L=89.62 in	performs worse than reconstructed envelope
Present transverse position	four Petrie clearance pairs	3.50–3.75° branch split across subsets
Same-survey L boundary	10 declared scalar substitutions	0/10 enter frozen slope envelope
Lost lid	flush state t=recess	exactly invariant; other thicknesses are sensitivities only
Natural cavity diagonals	four internal diagonals	do not replace external envelope role
Access route	ascending passage clearances	external width constrains movement, not h
Queen's finished gable	physical triangular control	approximately 30.50°, not exterior face

S13. Inserted-floor sensitivity and transferred operator (R08)

Removing the installed floor changes the free height and therefore the crossed-corner output. This is a construction sensitivity showing that the finished datum could affect the geometry; it is not evidence that intentional iterative tuning occurred. Applying the measured-face inverse to the Queen's Chamber gives a hypothetical object length near 19.10 in. This exterior-input calculation is distinct from the internal D=g transfer, which gives the wall-top and gable-apex outputs reported in S9. No coffer is preserved, so neither calculation is a homologous replication.

E UNCERTAINTY, LIMITS AND PROSPECTIVE TESTS

S14. Uncertainty model and reporting discipline

The historical record does not presently justify a standard-deviation model for W, H, h or L0. The intervals combine survey variation, corrected architectural quantities, surface irregularity and analyst-declared sensitivity bounds. Accordingly, the present analysis reports central residuals, bounded envelopes and conditional null frequencies, but no sigma statements. The central D=g prediction and the reduced proportional decoder are close enough that modern uncertainty-bearing survey is needed for conventional statistical discrimination.

The frequently quoted 1.69-mm difference between the D=g prediction and rounded morphology is not treated as a measurement uncertainty. Likewise, the exact 1.08509% frequency and its R10.1 Monte Carlo verification are conditional on the declared domains and tolerance and are not universal chance probabilities.

S15. Frozen longitudinal-envelope protocol

Protocol A remains numerically frozen from 5 August 2026. It was designed for the earlier measured-face inversion before D=g was identified and is not a model-specific confirmatory test of the new decoder. A blinded team reconstructs the maximum original external longitudinal envelope from a calibrated 3-D point cloud, without receiving W, H, h, exterior angle, B/100, Petrie's 90.60-in reconstruction or decision bands. The compatibility core remains 90.404–90.789 in and the broad envelope 89.750–91.412 in. The present analysis records the D=g point prediction 90.666542 in prospectively but does not change the frozen classification bands.

S16. Frozen original-position protocol

Protocol B remains the independent archaeological test of the original transverse centre. Eligible evidence is physical contact, wear, bedding, residue, depression traces or an explicit independent archival coordinate frame. The current position and any target-informed reconstruction are ineligible. The R10.1 ±14.65-mm structural semiwindow is a descriptive register criterion; it is not substituted for the separately frozen strict and broad archaeological decision bands.

S17. Interpretation limits

R12 is supplementary and non-scored. Petrie's contents–bulk equality was historically discussed but explicitly described by him as inexact; our use of exact equality is therefore only an idealised inverse criterion for the lost envelope. The calculation assumes a rectilinear mean-plane envelope and the bounded-domain frequency is conditional on declared ranges. It is not combined with R10.1 or R11 as an independent probability.

The results support a constrained metrological reconstruction conditional on D=g, the documented input roles and assumed centred placement. Original registration has not been independently recovered, so deliberate dimensional coordination is not established. Symbolic meaning, religious interpretation, the builders' terminology and any description of the profiles as a cipher require additional evidence. Shared metrology explains part of B/W≈44, and Petrie's h/W≈1/5 observation has historical precedence; the contribution is the reversible construction, its omitted solver outputs, its declared alternatives and its independent survey tests.

F REPRODUCIBILITY AND CLAIM MAP

S18. Executable analysis inventory

Table S10. Executable analysis inventory

Module	Purpose
R01	core reproduction, bounded inverse and central geometry
R02	30-role assignment audit
R03	expanded role/scale/target sensitivity

Module	Purpose
R04	fixed-n centesimal calibration
R05	positional branch-split ablation
R06	same-survey boundary, lid and subset sensitivity
R07	internal architectural controls
R08	inserted-floor and Queen’s Chamber transfer
R09	target-consistent reduced-baseline partial discrimination
R10.1	corrected five-panel specificity audit: rules, geometry, roles, position and comparisons
R11	exact integration of the frozen specific-target geometry null
R12	historical coffer contents–bulk balance; envelope-length inverse and conditional volume sensitivity
R13	retrospective joint length–height reconstruction, diagonal/seked identities, dependency audit and bounded sensitivity
R14	exploratory joint-rule comparison under common volume balance; polynomial enumeration and independent direct-function verification
R15	Exploratory seven-route comparison, joint bounds, displacement normalisation, vertical identifiability and historical source substitution
R16	Whole-grammar Hawara body-section control, root-density coverage and conditional lid-reference interval
R17	exploratory coefficient-budget extension and bounded-input ranking sensitivity

S19. Principal claim matrix

Table S11. Principal claim matrix

Claim	Evidence class	Result
Preserved internal dimensions decode L and theta	W,H,h plus D=g	Equations S3–S5; R10.1
Decoded L matches destroyed-envelope region	separate morphology-based reconstruction	90.6665 vs approximately 90.60 in
Decoded profile matches exterior	north-face survey	51.83787°; −23.7 arcsec
Rule is internally specific	frozen rule grammar	1 of 127 classes passes length at 0.2%; tangent adds no rejection
Specific target is conditionally uncommon	declared plausible-ratio null	1.08509% exact; 1.0828% Monte Carlo at 0.2%
Correct physical roles matter	32-role null	2 close; same width class
Position is a material register	Petrie clearances; R10.1	present position 16.7× outside 1% semiwindow
Complete reduced family not excluded	R09	angular branch outside core; centesimal branch inside
Hawara fails homologically	Petrie Hawara transverse dimensions	27.363° actual X; 24.972° D=g transfer
Original position remains unresolved	historical evidence audit	separate blinded protocol
Historical volume relation predicts original length	Petrie §§61,156; R12	L_V=90.583750 in; 0.41 mm from morphology; morphology state is 0.035864% from volume balance; non-scored

Claim	Evidence class	Result
Joint reconstruction recovers length and height	D=g plus ideal volume balance; retrospective shared-data extension	L*=90.655879 in; h*=41.277132 in; central residuals +1.42/−0.83 mm; Table S12 sensitivity
D=g retains its rank when height is reconstructed	same original grammar; common ideal volume condition; retrospective comparison	1 of 154 classes passes length at 0.2%; Table S13; full root classes in R14
Reciprocal slopes separate displacement and direction	Derived coordinate identity; level geometry	R15; no independent archaeological confirmation

S20. Supplementary file map

Supplementary Data 1 provides the complete R01–R09 code and data, corrected R10.1 code and data, R11 exact-null verification, the supplementary R12 historical volume-balance analysis and the retrospective R13 joint reconstruction and dependency diagnostic, plus the exploratory R14 joint-rule comparison, R15 reconstruction and registration audit, and R16 whole-grammar body-section and lid-reference audit. Supplementary Information, Parts II and III reproduce frozen Protocols A and B; copies and their machine-readable thresholds are also included in Supplementary Data 1. The frozen numerical specifications and original scientific scripts retain their version labels. The archive README records the current file layout and execution commands. R17 provides the exploratory expanded grammars, bounded-input rankings and independent central-root verification documented in S25.

S21. Joint reconstruction and dependency diagnostics (R13)

R13 was added on 29 September 2026 after the original survey comparisons and R12 results were known. It is a retrospective extension, not a preregistration or a new observation. The original R01–R12 scripts, R10.1 scoring rules and prospective protocols are unchanged. External coffer length and height and the north-face angle are omitted from the joint solver inputs and used only to compare its outputs.

Completing the D=g quadratic gives $(G+L)^2=G^2+W^2$. Thus L is the excess of the diagonal of a W-by-G rectangle over G (main Figure 2A). Under the same equality, $\tan\theta=14/11$ is equivalent to $r=11/25$ and $A=252/275$. The measured A differs from 252/275 by 0.0145988%, whereas $\sqrt{5}/2-1/5$ differs by 0.1822805%. These are identities and central-value comparisons, not additional observations.

For the joint model, $K=2l_iw_id_i/W_e=3742.014733$ in². Substitution of $h=K/L$ into $L^2+2(H-h)L-W^2=0$ gives the unique positive solution:

$$L_* = \sqrt{H^2 + W^2 + 2K} - H \quad \text{(S9)}$$

$$h_* = \frac{K}{L_*} \quad \text{(S10)}$$

The inputs are W=206.04, H=230.09, W_e=38.50, l_i=78.06, w_i=26.81 and d_i=34.42 in. The output is L*=90.655879422 in and h*=41.277132349 in, with $0<h^*<H$. A separate bisection in h reproduces the closed form to better than 10^{-10} in; substitution gives a D−g residual of 2.13×10^{-14} in and a zero volume residual at the stored precision. The derived θ*=51.843716746° is 2.6197 arcsec below the measured north-face central value.

Table S12. Joint reconstruction under declared chamber-dimension sensitivities

W (in)	H (in)	L* (in)	h* (in)	ΔL (mm)	Δh (mm)	Δθ (arcsec)
206.04	230.09	90.655879	41.277132	+1.419	-0.835	-2.62
206.12	230.09	90.707275	41.253744	+2.725	-1.429	-34.58
205.92	230.09	90.578807	41.312254	-0.538	+0.057	+45.32
206.16	230.09	90.732978	41.242058	+3.378	-1.726	-50.55

W (in)	H (in)	L* (in)	h* (in)	ΔL (mm)	Δh (mm)	Δθ (arcsec)
206.04	229.94	90.698293	41.257830	+2.497	-1.325	-86.34
206.04	230.24	90.613500	41.296437	+0.343	-0.344	+81.02
205.92	229.94	90.621195	41.292931	+0.538	-0.434	-38.39
205.92	230.24	90.536454	41.331580	-1.614	+0.548	+128.95
206.16	229.94	90.775417	41.222777	+4.456	-2.215	-134.28
206.16	230.24	90.690573	41.261342	+2.301	-1.236	+33.09

The first row uses the primary inputs; the second uses chamber-mean W. Remaining rows use the existing R01 bounds W=205.92–206.16 in and H=229.94–230.24 in, separately and at all four corners. ΔL is relative to L0=90.60 in, Δh to h=41.31 in, and Δθ to 51°50′40″. Coffer width and cavity dimensions remain fixed. These scenarios do not propagate every input uncertainty and are not confidence intervals. In particular, the central 2.62-arcsec agreement is not stable over the declared H range.

For the primary D=g decoder with h fixed, changing W to 206.12 in gives L=90.725533 in, 1.498 mm above its primary value and 3.189 mm above L0. H=229.94 and 230.24 in give shifts of +1.237 and −1.236 mm, respectively. The complete six-scenario output is R13/data/primary_sensitivity.csv.

In the original 127-class panel, the 0.2% length criterion accepts L in [90.418800, 90.781200] in. The tangent criterion, evaluated as 2(H−h)/(W+L), accepts [90.004388, 91.190939] in. The first interval is contained in the second; the pass counts are therefore one for length, three for tangent and one for both. Across the classes, eθ/eL ranges from 0.239056 to 0.383679. The external face is a distinct measured quantity, but the second acceptance criterion does not further narrow the length-selected set. The count 1/127 establishes uniqueness within the grammar and is not assigned a chance probability.

The joint reconstruction inherits the two assumptions already evaluated in R10.1/R12: D=g and an ideal rectilinear contents–bulk balance. Its height recovery makes their compatibility explicit but does not supply an independent confirmation. R13 is non-scored and does not change the rule ranking, null frequencies or frozen survey protocols. Its numerical script, exact outputs and Figure 2 source are in Supplementary Data 1.

S22. Rule selection with reconstructed external height (R14)

R14 was specified on 29 September 2026 after the original grammar results and R13 joint solution were known. It is an exploratory extension of the existing model. The original frozen grammar, thresholds and results remain unchanged; the extension asks whether D=g retains its selection when every expression receives the same ideal volume condition, h=K/L, and measured external height is withheld from solving.

All 1,950 original expressions and the 13 segment definitions are retained, with h=K/L substituted throughout and K=3742.014733090909 in² fixed by the measured cavity dimensions and external width. Multiplication by the positive common denominator 2L(W+L) produces polynomials of degree at most three. Coefficients use exact rational arithmetic. Exact identities and constant residuals are excluded, all real roots in 30<L<W−30 in are retained, and roots are grouped using the original rounding convention. Reported classes are ordered by length residual. The original fixed-height enumeration reproduces all 127 archived classes before the extension is evaluated.

The joint panel has 16 tautologies, 39 constant residuals, 559 admissible expression-root instances and 154 distinct classes. The smallest separation between classes is 0.004683 in, well above the 0.0001-in grouping resolution. D=g remains first and is the only class with length error at or below 0.2%. It also meets the height threshold; that criterion adds no rejection at the central inputs. Table S13 gives the five nearest length classes. The complete class table, including every equivalent expression, is R14/joint_all_classes.csv.

Table S13. Leading classes under the common ideal volume condition

Rule class	L (in)	h (in)	Length error (%)	Height error (%)
D=g	90.655879	41.277132	0.061677	0.079563

Rule class	L (in)	h (in)	Length error (%)	Height error (%)
H=2(W−L)	90.995000	41.123301	0.435982	0.451947
L=U−h	89.425862	41.844883	1.295958	1.294802
U=3L/2	87.646709	42.694298	3.259703	3.351000
G/2=g+h	94.608226	39.552742	4.424090	4.253832

Errors are absolute fractional differences from L0=90.60 in and h0=41.31 in, expressed as percentages. They share the condition Lh=K and are not independent confirmations. The count 1/154 reports selectivity within this extended grammar, not a chance probability. These results use central inputs; the existing R13 sensitivity scenarios remain applicable, and the panel does not establish ranking stability over all input bounds.

A separate implementation evaluates the original segment functions directly, brackets roots and solves them with Brent's method. It reproduces all 559 admissible root instances and all 154 classes, with a maximum root difference of 3.41×10^{-13} in and maximum direct equation residual of 2.42×10^{-13} in. These tolerances describe numerical agreement, not survey precision. R14 contains the extension protocol, both scripts, the original input specification and class table, complete output tables and verification report.

S23. Exploratory reconstruction and registration audit R15

This analysis was added on 13 October 2026 after the original results were known. It is exploratory and retrospective; it neither modifies the R01–R14 rules nor redefines the frozen survey protocols. The seven routes below have different information budgets. Reported angles embed each calculated length in the same measured section, $\theta=\operatorname{atan}[2(H-h)/(W+L)]$. For the reduced-proportion route this embedding angle differs from the route's idealised native angle. No residuals are combined into a probability or a universal model ranking.

Table S14. Reconstruction routes embedded in the measured section

Route	L in	ΔL mm	Δθ arcsec
D=g	90.666542	+1.690	-23.67
11/25 proportional length	90.657600	+1.463	-20.65
Reduced-proportion D=g	90.546071	-1.370	+17.03
Ideal volume balance	90.583750	-0.413	+4.30
Measured-face inversion	90.596477	-0.089	+0.00
Nominal seked inversion	90.614286	+0.363	-6.02
B/100	90.688000	+2.235	-30.91

ΔL is relative to Petrie's approximate 90.60-in morphological estimate; Δθ is relative to his north-face central angle. Measured-face inversion inserts that angle. Nominal-seked inversion inserts exterior tangent 14/11. B/100 inserts the measured exterior base. The 11/25 length assumes a ratio; the reduced route imposes Petrie's ideal H/W and h/W proportions within D=g; volume balance uses the cavity, coffer width and measured height. All routes are retrospective. Several alternatives have smaller central residuals than the primary decoder; this does not establish historical superiority or statistical separation.

Using $W\in[205.92,206.16]$, $H\in[229.94,230.24]$ and $h\in[41.14,41.50]$ in, already declared in R01, simultaneous endpoint combinations give $L_{Dg}\in[90.474420,90.865530]$ in and angular residuals

from −312.08 to +251.43 arcsec. Monotonicity makes these exact extrema on the rectangular input box: L increases with W and h and decreases with H; the angle increases with (H−h)/W. These bounds do not supply a probability distribution or a confidence interval.

For a level, unrotated section with $a=(W+L)/2$, $t_1=G/(a+\delta)$ and $t_2=G/(a-\delta)$, the identity $1/t_1+1/t_2=(W+L)/G$ gives the centred tangent through its reciprocal sum. This is an elementary restatement of the endpoint geometry; it supplies no independent match or evidence of original centring. Recovering δ from the reciprocal contrast additionally requires the known scale a, hence W and L. The coordinate checks in R15 verify the numerical implementation of these identities.

In a common vertical frame, $G=Z_{ceiling}-Z_{coffer_top}=H-h-z$. A change of coordinate origin cancels exactly. Physical lifting, a changed ceiling elevation or a changed coffer height affects the same clearance and cannot be distinguished from profile geometry alone. For $L=\sqrt{(W^2+G^2)}-G$, $\partial L/\partial W=W/\sqrt{(W^2+G^2)}=0.737315$ and $\partial L/\partial G=G/\sqrt{(W^2+G^2)}-1=-0.324450$ at the primary inputs. Independent surface and elevation observations are required to distinguish these causes.

As a conditional inverse diagnostic, D=g and an independently specified L imply $z=H-h-(W^2-L^2)/(2L)$. With central W,H,h, the approximate morphological L0 implies z=−5.21 mm, the volume-derived L implies −6.49 mm, and the surviving length implies −82.73 mm. These are conditional geometric requirements, not evidence of a recessed installation. They inherit uncertainty in the envelope and vertical references and must not be used to adjust the datum for agreement.

Smyth’s original tables were inspected visually at printed pp. 101, 102 and 119 of volume II (PDF scan pp. 173, 174 and 203). He reports mean chamber height 230.1 in above a disturbed floor, mean breadth 206.3 in, a single west-side breadth reading of 206.3 in, intrinsic coffer height 41.27 in, and a conjectural underside correction to 41.17 in. The observed-height substitution gives L=90.842056 in and θ=51.804409° (+6.148 mm; −144.126 arcsec against Petrie’s central comparisons). Its relative length residual is 0.267170%, exceeding the 0.2% comparison threshold used in R10.1. The conjecturally corrected height gives L=90.809584 in and θ=51.822192° (+5.323 mm; −80.107 arcsec), with length residual 0.231329%, also above 0.2%. Both angular residuals lie outside the ±65-arcsec north-face band. Neither source substitution reproduces the primary agreements; neither is an equivalent-datum replication. Smyth’s 89.71-in surviving mean length is not an original-envelope reconstruction. Both height conventions are retained without selection for fit.

To attribute the numerical change explicitly, start with the primary Petrie-input decoder and replace W, then H, then h with Smyth’s values. The exact contributions to L are +4.870626, −0.082526 and −0.330053 mm. Added to the primary +1.690174-mm residual, they give +6.148222 mm. This sequential decomposition is order-dependent for a nonlinear decoder, but identifies the dominant width contribution in this declared path. It does not establish that width endpoint or floor-datum differences historically caused the divergence, and does not justify adjusting either survey for fit.

The diagonal construction $L=\sqrt{(W^2+G^2)}-G$ is already established in R13. It permits a geometric sequence: determine the vertical clearance G; construct a rectangle with sides W and G; obtain its diagonal C; transfer G along C to obtain C−G; and centre the resulting length if testing symmetric registration. This is mathematical constructibility. R15 makes no claim that a particular ancient instrument, procedure or construction sequence has been archaeologically demonstrated.

R15 contains the standalone audit script, source provenance register, seven-route comparison, corner sensitivities, position-normalisation examples, conditional vertical requirements, source-substitution outputs and numerical verification. The original scientific files and frozen protocols remain unchanged.

S24. Whole-grammar body-section control and lid reference R16

R16 was specified and executed on 13 October 2026 after the Khufu results were known. It retains the 13-segment vocabulary and all 1,950 expressions. Multiplication by positive W+L gives polynomials of degree at most two; all admissible real roots are checked in the direct segment functions. The independent polynomial calculation reproduces all 127 stored original Khufu class lengths exactly at six-decimal resolution and all 476 root instances. The original domain, $30<L<W-30$ in, is retained alongside an added proportional sensitivity, $30/206.04<L/W<1-30/206.04$. Original thresholds, class grouping and R01–R15 outputs are unchanged.

Hawara uses the documented transverse body section W=94.2, H=92.4, h=55.5 in and measured coffer width 48.4 in (Petrie 1890, §§25–26). The unknown is transverse width, not longitudinal length. The whole grammar generates 69 classes in the original domain and 131 in the proportional domain; neither has a length match within 0.2%. The nearest length class in both domains is L=2U, giving 48.662049 in and 0.541423% error. With G=36.9 in, $\theta=\operatorname{atan}[2G/(W+L)]$ has supremum $\operatorname{atan}(2G/W)=38.076551$ degrees for positive L. The three casing fragments reported in §17, 48.75, 49.85 and 52.416667 degrees, are above the body-section ceiling. The angular ceiling rules out recovery of Hawara's exterior slope by this body-section construction; discrimination within the transferred grammar therefore rests on the measured-width criterion. They are alternative exterior references for one monument, not three independent controls. The lid, documented as 14.1 in deep with a curved top, is not substituted as a flat rectangular body top.

For a hypothetical target dimension uniform over the admissible interval, R16 computes the union of all root acceptance intervals [L_pred/1.002,L_pred/0.998], clipped to that interval. Coverage is 29.152230% for Khufu, 31.281166% for Hawara in the original domain and 29.757319% in the proportional domain. These quantities describe conditional root density; they are neither empirical monument false-positive rates nor likelihood ratios. Hawara is the single admissible external body-section control in this audit. The source and eligibility registers keep Khafre's gabled roof and embedded coffer, Menkaure's barrel roof, and unresolved Dahshur candidates outside the negative-control denominator. Their evaluation requires a separately declared endpoint/datum convention and adequate measurement records; no negative outcome is assigned to them.

The Khufu lid audit retains W=206.04, H=230.09, body h=41.31 in and zero base elevation. With ledge depth r=1.70 in (Petrie 1883, §59), a level parallel lid has $h_{eff}=h-r+t$, where t is effective thickness above its seating surface at the crossed endpoints, rather than necessarily the maximum central thickness. A flush lid t=r reproduces the body output exactly. Inverting $L=\sqrt{W^2+(H-h_{eff})^2}-(H-h_{eff})$ over the existing 0.2% length interval [90.4188,90.7812] in gives t=[0.934672,2.053017] in, or [23.740669,52.146622] mm. Relative to the body top, this is [−19.439331,+8.966622] mm. The central 90.60-in target gives t=1.494781 in. A hypothetical t=3 in gives L=91.089977 in, +12.445412 mm from that target and 0.540813% error. The derivative $dL/dh_{eff}=0.324450$ near the body inputs is checked through the exact scenarios. The body-top relation remains the primary geometric definition; a lid surface is a distinct reference state. No lid measurement for Khufu is supplied or inferred as historical fact.

Petrie §57 describes local sawing and drilling errors, not two global abandoned and final coffer lengths. It is not used as evidence of dimensional redesign. R16 contains both implementations, complete root-class tables, comparison summaries, lid scenarios and inverse interval, the preserved Khufu reference table, source and eligibility registers, and file hashes. Run audit.py and then verify.py separately; the main reproduce_all.py retains the original R01–R14 execution scope.

S25. Exploratory grammar expansion and input sensitivity R17

R17 is a retrospective extension dated 27 October 2026. It preserves the 13 physical segments, $30<L<W-30$ in domain, comparison quantities and root-equivalence convention of R10.1. Relations use two or three distinct segments with non-zero integer coefficients, identified up to an overall sign and reduced by their coefficient greatest common divisor. Every sign and term placement is considered; all-positive sums are excluded because physical segment lengths are positive. The coefficient budget is the sum of absolute coefficient values and is defined relative to this vocabulary, not as a universal measure of geometric complexity. The complete qualifying and non-qualifying classes are archived.

Budget three gives the same 127 fixed-height root classes as R10.1 despite fewer syntactically duplicated expressions. Budget four increases this to 338 classes while retaining D=g as the sole length match at 0.2%. Budget five gives 686 classes and retains D=g as the closest central length prediction, but introduces another qualifying relation, $3L=H+h$. Its $L=90.466667$ in differs from the 90.60-in morphology target by -3.386667 mm (0.147167%); its crossed-section tangent residual is 0.043780%. Thus the extended comparison preserves central preference but bounds the exclusivity claim. Table S15 reports both length-only and paired criteria.

Table S15. Central fixed-height rule classes under expanded coefficient budgets.

Search	Expressions	Classes	Length passes	Length and tangent passes	D=g length rank
Original R10.1	1,950	127	1	1	1
All orientations, budget ≤3	1,092	127	1	1	1
Budget ≤4	3,822	338	1	1	1
Budget ≤5	9,282	686	2	2	1

All passes in Tables S15–S16 use the existing 0.2% relative criteria. Central ranking here is explicitly by absolute length residual, whereas the original R10.1 descriptive worst-channel ranking remains unchanged. The angle remains a deterministic function of L at fixed W,H,h. Central class counts do not define chance probabilities.

With the same volume constraint $Lh=K$ imposed on every rule, budgets four and five yield 432 and 897 joint classes. D=g remains the best central length fit in both; respectively one and three classes satisfy both length and height criteria (Table S16). The alternative $3L=H+h$ leads to $3L^2-HL-K=0$ and gives $L=90.482132$ in and $h=41.356395$ in, with respective errors of 0.130098% and 0.112308%. As in R14, the shared volume constraint makes the output errors dependent; this is not independent replication.

Table S16. Joint rule classes under the common ideal volume constraint.

Search	Classes	Length and height passes	D=g length rank
Original R14	154	1	1
Budget ≤4	432	1	1
Budget ≤5	897	3	1

The bounded-input audit evaluates 21 equally spaced values of W on [205.92,206.16], H on [229.94,230.24] and h on [41.14,41.50] in, giving 9,261 combinations. The historical morphology target is held at 90.60 in. All admissible roots of every equation are recomputed at each point, rather than merely shifting the central class representatives. Consequently the central counts identify families, not a fixed number of roots at every grid point. Table S17 separates length ranking from threshold acceptance.

Table S17. Deterministic sensitivity of length ranking and alternative acceptance.

Rule family	D=g first	Any alternative within 0.2%	Minimum D=g advantage (mm)
Original grammar	9,261 / 9,261	0 / 9,261	+1.890
Budget ≤4	9,238 / 9,261	214 / 9,261	−1.468
Budget ≤5	4,998 / 9,261	9,222 / 9,261	−4.858

Advantage is the nearest alternative's absolute length error minus the D=g error; a positive value favours D=g. In the original grammar D=g passes the length criterion at 8,712 points, while the other 549 points have no qualifying rule. Its length range is [90.474420,90.865530] in. At budget four, 23 grid points favour an alternative. The most adverse point has W=206.16, H=229.94 and h=41.14 in, where W/2+G/2=2Y gives L=90.509268 in versus 90.748539 in from D=g. At budget five, additional alternatives reduce ranking stability further. These counts describe the specified deterministic grid, not confidence probabilities, observed monument frequencies or certification over the continuous input box.

At central inputs, the original grammar's neighbouring roots bound the target interval over which D=g remains the nearest prediction: 90.360434–90.830771 in. This is a nearest-root interval for a varying comparison target, not a morphometric uncertainty interval. All broader physical claims retain the independent envelope and original-position requirements of S15–S17. In particular, the maximum longitudinal extent of the ideal rectangular body must be distinguished from surviving mean-plane length, skewed end-face spans and rotational projection effects; the numerical comparison does not supply a shape correction.

Verification evaluates the 13 explicit segment functions using exact rational polynomial interpolation, a separate companion-root solver and Brent refinement. It reproduces all central classes in the original and expanded fixed-height and joint searches: 127, 154, 338, 432, 686 and 897. The maximum direct-function residual is 8.53×10^{-13} in and the largest root difference is 3.55×10^{-13} in; these are numerical checks, not archaeological precision estimates. The grid calculations are supplied in full but are not independently certified over the continuous domain. Run R17/audit.py and R17/verify.py; original source files, thresholds and frozen protocols remain unchanged.

REFERENCES

Cole, J. H. 1925. Determination of the exact size and orientation of the Great Pyramid of Giza. Survey of Egypt Paper 39. Cairo: Government Press.

Gillings, R. J. 1972. Mathematics in the time of the Pharaohs. Cambridge, MA: MIT Press.

Nell, E., and C. Ruggles. 2014. The orientations of the Giza pyramids and associated structures. Journal for the History of Astronomy 45 (3): 304–360. https://doi.org/10.1177/0021828614533065.

Petrie, W. M. F. 1883. The pyramids and temples of Gizeh. London: Field & Tuer.

Petrie, W. M. F. 1890. Kahun, Gurob, and Hawara. London: Kegan Paul, Trench, Trübner.

Robins, G., and C. C. D. Shute. 1987. The Rhind mathematical papyrus: An ancient Egyptian text. London: British Museum Publications.

Rossi, C. 2004. Architecture and mathematics in ancient Egypt. Cambridge: Cambridge University Press. https://doi.org/10.1017/CBO9780511550720.

Smyth, C. P. 1867. Life and Work at the Great Pyramid during the Months of January, February, March, and April, A.D. 1865. Vol. II. Edinburgh: Edmonston and Douglas, pp. 101–102, 119.

Frozen prospective protocol for a blinded 3-D reconstruction of Khufu's sarcophagus original envelope

Version 1.0 | Frozen 5 August 2026 | Unchanged numerical rules, packaged with Version 7.5

Prospectively fixed before inspection of any new 3-D scan or morphometric reconstruction

1. Purpose and scope

This protocol adjudicates one claim: whether a morphometric reconstruction based solely on the damaged sarcophagus supports the original external longitudinal envelope predicted by the King's Chamber–exterior construction. It does not test symbolic intention, authorship, date or the arithmetic correctness of calculations made from Petrie's published central values.

2. Frozen endpoint and numerical bands

Primary endpoint: the maximum original external longitudinal envelope Lmorph, reconstructed from the sarcophagus point cloud and damage morphology without using chamber or exterior-pyramid dimensions.

Item	Frozen value
Angle-route central prediction	90.59647664 in
Petrie B/100 route	90.688 in
Compatibility core	90.404–90.789 in
Broad conservative envelope	89.750–91.412 in

3. Eligible data

- A metrically calibrated 3-D point cloud or surface mesh covering both damaged ends, both preserved long faces, the external top and enough internal surface to identify orientation.
- Raw and processed data archived with scale calibration, scanner specification, registration report and all transformations.
- Coverage sufficient to define the longitudinal axis and estimate both missing end envelopes; omission of either damaged end makes the primary endpoint ineligible.
- No reconstruction previously fitted with chamber dimensions, exterior-pyramid dimensions, B/100 or the 90.60-in target is eligible as the primary analysis.

4. Blinding

A data curator provides calibrated geometry and the physical endpoint definition. Until analysis lock, the morphometric team is not provided W, H, h, θface, Lθ, B/100, Petrie's approximate original length or the decision bands. Before unblinding, the team deposits a timestamped report, executable code, all exclusions and masks, model-specific and combined estimates, uncertainty intervals and SHA-256 hashes.

5. Coordinate system and estimator

The longitudinal axis is estimated from a joint robust fit to the preserved external long-face surfaces. Damage masks are defined before missing-surface reconstruction. The external envelope is reconstructed at both ends; the primary endpoint is the maximum distance between reconstructed original end envelopes along the frozen longitudinal axis.

At least three predeclared reconstruction families are reported: a low-order polynomial surface, a regularised spline and a Gaussian-process or equivalently uncertainty-bearing smooth surface. The primary point estimate is the median of eligible model-specific envelope estimates. The primary 95% uncertainty interval is the union of model-specific bootstrap or posterior 95% intervals. No family is discarded because its result is distant from the prediction.

6. Quality-control gates

Gate	Pass rule	Failure consequence
Registration	Global registration RMSE ≤1.0 mm	Re-register or reacquire before endpoint opening
Held-out reconstruction	Median absolute error ≤2.0 mm	Primary classification invalid
Held-out tail error	95th-percentile absolute error ≤5.0 mm	Primary classification invalid
End coverage	Both damaged ends and long-face curvature represented	Endpoint ineligible
Locked analysis	Report, code, exclusions and hashes deposited before unblinding	Result exploratory only

7. Frozen primary decision rule

Classification	Rule
Compatible	Point estimate in 90.404–90.789 in AND 95% interval wholly in 89.750–91.412 in.
Incompatible	95% interval wholly below 89.750 in OR wholly above 91.412 in.
Indeterminate	Every other outcome, including intervals that cross a boundary or fail to resolve the core.

The bands were frozen before the Version 7.5 positional audit and are not recalculated after new morphology is observed. The compatibility core is the angle-only inverse range; the broad envelope combines the conservative historical bounds on angle, chamber width, chamber height and sarcophagus height.

Post-freeze interpretive note added in Version 7.5; thresholds and decision rules are unchanged. On the measured-face scale, the core excludes the reduced H/W, h/W angular branch at 91.181 in but includes the reduced centesimal branch at 90.658 in. This is partial directional discrimination only: the protocol was not frozen as a full-model comparison, and the broad envelope includes both branches.

8. Secondary tests

Branch asymmetry: independent northwest and southwest reconstructions are compatible only when each branch's 95% slope interval overlaps 1.269982–1.275462 and the two branch intervals overlap one another. If either interval lies wholly outside the band, the symmetric-X extension is incompatible; otherwise it is indeterminate.

Original-position reconstruction is governed by a separate frozen protocol. It cannot rescue an incompatible envelope endpoint and is not included in the primary longitudinal decision.

9. Exclusions and deviations

- No chamber dimension, pyramid dimension, B/100 value or historical 90.60-in target may enter surface fitting.
- All predeclared model families and model-specific outputs are retained; selective reporting is prohibited.
- Surface masks, smoothing parameters, coordinate transformations and outlier rules are frozen before unblinding.
- Protocol deviations are timestamped before unblinding and do not alter the frozen decision bands.
- An analysis failing quality-control or blinding is labelled exploratory and cannot produce a confirmatory classification.

10. Interpretation and impact rule

A compatible result strengthens the claim that the chamber–exterior operator recovers the damaged original envelope, but does not prove symbolic intention. An incompatible result retires that recovery claim and any argument depending on it. It does not alter the direct arithmetic fact that Petrie's printed central measurements generate the reported X angle. An indeterminate result produces no directional evidential update.

11. Freeze record

Machine-readable thresholds accompany this protocol in data/frozen_prospective_thresholds_v7_5.csv and data/frozen_prospective_protocol_v7_5.json. The protocol, data files and code are included in the Version 7.5 SHA-256 manifest.

Frozen prospective protocol for Khufu's sarcophagus original transverse position

Version 1.0 | Frozen 5 August 2026

Fixed after historical-source audit and before inspection of new confirmatory positional evidence

1. Purpose and inferential scope

This protocol adjudicates whether the original north–south centre of Khufu's sarcophagus was sufficiently close to the reconstructed chamber centreline to realise the equal-angle physical X. It does not use the X to infer the position and does not treat the current measured placement as original.

2. Frozen endpoint and bands

Primary endpoint: δ0, the original transverse centre offset of the reconstructed sarcophagus envelope relative to the reconstructed upper west-wall centreline. Positive values denote a southward offset.

Item	Frozen value
Current correction from Petrie clearances	9.64875 in southward
Ideal equal reconstructed gap	57.720 in north and south
Strict compatibility core	−0.09447 to +0.09447 in
Broad positional envelope	−0.31084 to +0.31084 in

3. Eligible confirmatory evidence

- Direct contact, wear, bedding, residue or depression traces tied metrically to the chamber walls and shown to predate modern disturbance.
- A calibrated 3-D reconstruction resolving the chamber floor, sarcophagus base, tilt, current supports and candidate earlier contact surfaces.
- An independent archival survey reporting explicit original-position offsets to chamber walls.
- Any physical or documentary trace must define an uncertainty interval for δ0.

4. Ineligible evidence

- The current position alone.
- A centred placement selected because Equation (1) requires it.
- A drawing without chamber-wall coordinates.
- The exploratory near-45° translation or any modular east–west target.
- An analysis that receives the target bands before masks, exclusions, code and uncertainty are locked.

5. Blinding and analysis lock

The analyst receives the eligible positional evidence and coordinate definitions but not the strict/broad bands, the 9.64875-in current correction or the model's desired centre. Before unblinding, the analyst deposits data masks, exclusions, coordinate transformations, code, point estimate, 95% interval and SHA-256 hashes.

6. Frozen decision rule

Classification	Rule
Compatible	$\|\delta 0$ point estimate$\| \le 0.09447$ in and the 95% interval lies wholly within ± 0.31084 in.
Incompatible	The 95% interval lies wholly north of -0.31084 in or wholly south of $+0.31084$ in.
Indeterminate	No surviving trace, insufficient precision, an interval crossing a boundary, or any other outcome.

7. Impact rule

A compatible result upgrades transverse centring from a model condition to supported original placement. An incompatible result retires the interpretation of a physically realised symmetric X. An indeterminate result leaves the Version 7.5 construction as an idealised original-state reconstruction. No positional outcome changes the descriptive arithmetic obtained from Petrie's published central dimensions.

8. Freeze record

Machine-readable thresholds and the full evidence-classification record accompany this protocol in data/frozen_original_position_thresholds_v7_5.csv and data/frozen_original_position_protocol_v7_5.json. The package SHA-256 manifest fixes this protocol before inspection of any new confirmatory positional evidence.